Journal of Materials Chemistry C

ROYAL SOCIETY OF CHEMISTRY

PAPER

View Article Online
View Journal | View Issue

Cite this: J. Mater. Chem. C, 2025, 13, 22712

Influence of $K_4Nb_6O_{17}$ secondary phase on ferroelectric behavior of $K_{0.5}Na_{0.5}NbO_3$ thin films

B. Carreño-Jiménez, *[a] H. Kuentz, [ab] K. Kpoton, [a] T. Rotrou, [b] S. Ollivier, [a] V. Demange, [a] L. Joanny, [a] L. Rault, [a] G. Taupier, [a] B. Gautier, [c] G. Le Rhun [b] and M. Guilloux-Viry *[a]

$K_xNa_{1-x}NbO_3$ (KNN) perovskite thin films deposition by various methods poses significant challenges due to alkali cations losses, which result in vacancies or secondary phases. In this study, KNN thin films were obtained by pulsed laser deposition using a stoichiometric commercial target and a 60% potassium-enriched target on platinized silicon substrates. Potassium-enrichment target was used as an alternative to obtain a pure perovskite phase and enhance piezoelectric and ferroelectric behavior of the thin films. It was observed that the alkali losses during the deposition of KNN thin films mainly promote the formation of the secondary phase $K_4Nb_6O_{17}$ and its hydrated form. Importantly, $K_4Nb_6O_{17}$ adversely affects ferroelectric and piezoelectric properties owing to its high sensitivity to moisture. It was observed that these KNN films grown from a stoichiometric commercial target (denoted as KNNs) present a perovskite structure and $K_4Nb_6O_{17}$ secondary phase presence, while thin films deposited with a K-enriched target (denoted as KNNe) show a single perovskite structure. The topography and piezoresponse force microscopy amplitude exhibit topographic differences and a null-piezoelectric response in large and flat grains in KNNs, disrupting the distribution of small and rounded grains associated with piezoelectric signal. Meanwhile KNNe films present strong piezoelectric behavior. Null-piezoelectric response in KNNs agree with scanning electron microscopy and energy-dispersive X-ray spectroscopy analysis, where areas exhibiting such large and flat grains displayed a pronounced deficiency in alkali cations. In addition, characterization by using X-ray diffraction, Raman spectroscopy, scanning and transmission electron microscopy coupled to energy dispersive X-ray spectroscopy showed the presence of low amount of sodium incorporated into the $K_4Nb_6O_{17}$ structure during KNN films deposition, although only the $K_4Nb_6O_{17}$ was reported. On the other hand, thin films deposited from a K-enriched target presents a single perovskite phase devoid of any secondary phase. Their electrical measurements, performed on 0.25 × 0.25 mm^2 capacitors, show a $d_{33,f}$ value ~40 pm V^{-1} and typical ferroelectric behavior with saturation polarization = 20 μC cm^{-2}, remnant polarization ($2P_r$) = 17.5 μC cm^{-2} and coercive voltage ($2V_c$) = 3 V, comparable to earlier works reported in the literature, making KNNe thin films suitable candidates for further engineering applications through their optimization, contrary to KNNs thin films.

Received 24th July 2025,
Accepted 9th October 2025

DOI: 10.1039/d5tc02808f

rsc.li/materials-c

1. Introduction

$K_xNa_{1-x}NbO_3$ (KNN) thin films have a wide applicability in diverse microelectromechanical systems (MEMS). Their ferroelectric and piezoelectric properties which are attractive to use in sensors, actuators or transducers in diverse fields encourage the growing research.[1–3] As a potential alternative to $PbZr_xTi_{1-x}O_3$ type materials the lead-free KNN ceramics present a perovskite structure with an orthorhombic crystallographic phase at room temperature, and a high thermal stability due to its Curie temperature around 400 °C.[4] Some electrical characterizations of $K_{0.5}Na_{0.5}NbO_3$ thin films reported in the literature shows a P_r = 12.6 μC cm^{-2}, P_{sat} = 25.0 μC cm^{-2}, and $d_{33,f}$ = 58 pm V^{-1} of films deposited by PLD on Pt/Si(100),[1] P_r = ~40 μC cm^{-2} of textured films deposited by PLD on $SrRuO_3/SrTiO_3$(001),[5] $d_{33,f}$ = 30 pm V^{-1}, and P_r = 2.34 μC cm^{-2}, of films deposited by spin-coating on Pt/Si(100).[6,7] However, the formation of secondary phases during the deposition of KNN thin films is still a critical challenge that significantly affects their piezoelectric performance. Some secondary phases, such as $K_6Nb_{10.9}O_{30}$, $K_2Nb_8O_{21}$, $K_2Nb_4O_{11}$ and

[a] Univ Rennes, CNRS, ISCR – UMR 6226, ScanMAT – UAR 2025, F-35000 Rennes, France. E-mail: brenda.carreno@univ-rennes.fr, maryline.guilloux-viry@univ-rennes.fr
[b] CEA-Leti, Univ. Grenoble Alpes, F-38000 Grenoble, France
[c] INSA Lyon, CNRS, Ecole Centrale de Lyon, Université Claude Bernard Lyon 1, CPE Lyon, INL, UMR 5270, F-69621 Villeurbanne, France

$K_4Nb_6O_{17}$, have been reported in KNN thin films deposited by pulsed laser deposition (PLD) varying the oxygen pressure or temperature, as well as films obtained by chemical solution deposition.[8–11] Among the most commonly reported secondary phases, whose phase is close to perovskite according to the K_2O–Nb_2O_5 phase diagram,[12] $K_4Nb_6O_{17}$ is particularly detrimental. Its presence disrupts the perovskite structure of KNN and increases dielectric losses and reduces ferroelectric and piezoelectric responses. Structurally, $K_4Nb_6O_{17}$ shares some similarities with KNN, as exhibit NbO_6 octahedron. However, while KNN crystallizes into a perovskite structure with a long-range ordered ferroelectric domain arrangement, $K_4Nb_6O_{17}$ adopts a layered structure, which consists of corner- and edge-sharing NbO_6 octahedra in layers and the K^+ ions are located between the layers to compensate for the negative charges.[13,14] Some studies of its electrical properties on single crystal have shown a lack of ferroelectric and piezoelectric activity.[15–17] Consequently, the presence of $K_4Nb_6O_{17}$ secondary phase in KNN thin films hinders domain alignment and charge transport, resulting in degraded electrical properties. In addition, it has been reported that $K_4Nb_6O_{17}$ is highly sensitive to moisture, since it has been observed that if it is exposed to an environment with humidity between 25 and 85% it easily hydrates to become $K_4Nb_6O_{17}$–$3H_2O$.[18] Specifically, when using physical vapor deposition methods, such as PLD, it is necessary to consider that secondary phases are influenced by targets features, substrate temperature, oxygen pressure and fluence. In literature, some approaches have been studied to avoid secondary phases, such as using K- or/and Na-enriched targets in sputtering deposition[19] and PLD,[20] or introduction of an alkali cations excess into the solution used for spin coating method,[21] which compensates for the alkali volatilization. For PLD method, K_2O particularly exhibits a higher tendency to evaporate compared to Na_2O due to its lower melting point (740 °C and 1132 °C, respectively) and its higher vapor pressure at elevating temperature.[2] Then, providing that suitable deposition parameters are used, PLD targets with only K-excess compensate well for the losses, stabilizing the perovskite phase during thin film growth.[23,24] In this work, the detrimental influence of the secondary phase $K_4Nb_6O_{17}$ presence on ferroelectric and piezoelectric performance of $K_{0.5}Na_{0.5}NbO_3$ thin films obtained by PLD was studied, analyzing their structural and microstructural characteristics as a resulting of the use of stoichiometric and enriched targets.

2. Experimental methods

2.1 KNN target sintering

$K_{0.5}Na_{0.5}NbO_3$ (KNN) thin films were obtained by pulsed laser deposition (PLD) using a commercial stoichiometric target provided by JX Nippon Mining & Metals and a K-enriched target fabricated in our laboratory. Ceramic powders synthesis was carried out by solid-state reaction. The reagents used were K_2CO_3 (99.0%, Acros Organics), Na_2CO_3 (99.8%, NORMAPUR®), and Nb_2O_5 (99.5%, Thermo Scientific), which were weighed in stoichiometric ratio and grounded in a planetary ball-mill at 400 rpm for 30 min. Subsequently, the mixture was pressed into a disk and calcinated at 940 °C for 4 h in air. Afterward, the target sintered by conventional method was prepared grounding the ceramic powders obtained from the previous calcination in a planetary ball-mill at 400 rpm for 30 min with a 60% KNO_3 (99%, Alfa Aesar) mol excess. Later, the mixture was compacted into a disk at 170 kg cm^{-2} and annealed in two stages: (1) 350 °C for 6 h; (2) 500 °C for 6 h. Despite achieving a low final density, these temperatures were deliberately chosen to take benefit of the low melting point of KNO_3, which enhances the strengthening of the target material and prevents potassium loss due to decomposition of KNO_3. For the commercial KNN target, the supplier reports a stoichiometric composition and high densification. Targets features are summarized in Table 1.

Table 1 Main features summary of the K-enriched and commercial KNN targets

Target	Enrichment of KNO_3 (%)	Average composition by SEM/EDXS	Relative density (%)	Details
1	60	$(K_{0.65}Na_{0.35})_{1.16}NbO_3$	~60	Conventional Sintering
2	0	$(K_{0.55}Na_{0.45})_{0.85}NbO_3$	~97	Commercial

2.2 KNN thin films deposition

The Pt/TiO_2/SiO_2/Si (100) substrates were prepared at CEA-Leti, where SiO_2/Si (100) wafers were successively coated with 20 nm TiO_2 and 100 nm Pt by sputtering. Then, KNN thin films deposition were performed at ISCR, using a KrF excimer laser (Coherent company, pulsed duration 20 ns, λ = 248 nm) with an energy laser of 210 mJ and 4 Hz frequency, under 0.3 mbar oxygen partial pressure, 55 mm substrate-target distance, and ~650 °C substrate temperature. It is important to remark that substrate dimensions were 10 × 20 mm^2, which is large for a standard small surface laboratory PLD. It has been observed that the homogenous area from a composition point of view is typically 10 × 10 mm^2, without the need for any movement of either the laser beam or the substrate during deposition. Therefore, in this work, the characteristics of the films were investigated on the whole surface in a combinatorial approach. Obtained thin films have been labeled through the paper as KNNe for thin films realized from the potassium enriched target sintered by conventional method, and KNNs thin films, which were deposited using the stoichiometric commercial target.

2.3 Characterization methods

KNN targets and thin films were characterized by X-ray diffraction (XRD) by using a θ–2θ diffractometer (D8 Advance, BRUKER) with a monochromatized Cu Kα_1 wavelength (λ = 1.54056 Å) to determine their crystallographic characteristics. XRD characterization was performed from 5° to 80° 2theta, 40 kV and 40 mA. The microstructural characterization of thin films was carried out by scanning electron microscopy (SEM, JSM 7100F, JEOL) and the average grain size was determined by ImageJ measuring the length of grains in different directions. The statistical analysis was carried out by Origin plotting the corresponding histograms and obtained the average grain size and their standard deviation. Composition

measurements of targets and thin films were performed by scanning electron microscopy with a coupled X-ray energy dispersive spectroscopy detector (SEM-EDXS, SDD X-Max 50 mm^2, Oxford Instruments). Transmission electron microscopy (TEM) was carried out by a LaB_6 JEOL JEM-2100HR instrument equipped with an EDXS Oxford Instruments X-Max 80 mm^2 SDD device. Samples preparation for TEM observation consists of scratching the surface of thin films with a diamond tip and collecting the particles on a carbon copper grid. Bright field and dark field transmission electron micrographs, and electron diffraction patterns were recorded by a GATAN Orius 200D CCD camera. Additional structural study was done by Confocal Raman Spectrometry using a LabRAM HR-Evolution spectrometer, Horiba Scientific. The size of analyzed zones was 60 × 60 μm^2, while mapping was performed with a 1 μm diameter laser beam in 10 μm steps using a laser wavelength of 532 nm, ~6 mW power, and a x100 objective. Deconvolution of Raman peaks was carried out by OriginLab, using a Gaussian peak function[25,26] and Levenberg Marquardt iterative algorithm. Piezoresponse force microscopy (PFM) was performed with an NTEGRA NT-MDT system using the so-called "Dual Frequency Resonant Tracking" mode, with an external Zurich Instrument HF2LI system. Platinum–iridium tips have been used, with stiffness in the 2–10 N m^{-1} range. Micro capacitors were prepared by successively depositing 5 nm of RuO_2 and 100 nm of Pt by sputtering and then patterning top electrodes *via* photolithography and dry etching steps. Ferroelectric and piezoelectric characterization were carried out by using the double beam laser interferometer (DBLI) coupled with the TF analyzer 2000 from aixACCT.

3. Results and discussion

3.1 X Ray diffraction analysis

Structural analysis of KNN thin films by XRD requires particular attention to the angular range 2θ examined due to the possible presence of the layered $K_4Nb_6O_{17}$ (JPCDS 04-010-2507, $P2_1nb$, a = 7.83 Å, b = 33.21 Å, c = 6.46 Å) and its hydrated form $K_4Nb_6O_{17}$–$3H_2O$ (JCPDS 00-21-1297, a = 7.85 Å, b = 37.67 Å, c = 6.46 Å) as secondary phases in the KNN films.[27,28] These phases are present when the films are potassium-deficient, in accordance with the K_2O–Nb_2O_5 phase diagram, which shows that the stable $K_4Nb_6O_{17}$ appears for slight potassium deficiency,[12] but when it is present in very small quantities, only the most intense 0k0 diffraction peaks are visible in the pattern at low angles in the diagram, *i.e.* around 5° for 020 and 10° for 040 reflections, respectively. For this reason, it is recommended to record XRD patterns from lower angles ($2\theta \sim 5°$) to verify the presence of the single perovskite phase in the films. Fig. 1(a) shows the XRD patterns with 2θ = 5° to 80° of KNNe and KNNs thin films obtained from an enriched and commercial stoichiometric target, respectively. In addition, the reflection positions of $K_{0.5}Na_{0.5}NbO_3$ (JPCDS 04-25-7609 $Amm2$, a_o = 3.9475 Å, b_o = 5.6267 Å, c_o = 5.6633 Å), $K_4Nb_6O_{17}$ and $K_4Nb_6O_{17}$–$3H_2O$ phase are included. The orthorhombic KNN phase can also be described with a pseudo-cubic lattice, *i.e.* $a_{pc} = a_o$ = 3.9475 Å, $b_{pc} = b_o/\sqrt{2}$ = 3.978 Å, $c_{pc} = c_o/\sqrt{2}$ = 4.004 Å.

KNNe thin films obtained with an enriched target present only the perovskite structure with peaks around 2θ = 22.4°, 45.9° and 70.6° corresponding to a preferential $(001)/(010)_{pc}$ orientation (marked by a dashed line) induced by the crystallographic characteristics of the $Pt/TiO_2/SiO_2/Si(100)$ substrate. This preferential orientation can be confirmed from the intensity ratio of the (001) orientation with respect to (110), where I_{110}/I_{001} = 0.02. Structurally, it has been reported that the KNN thin films with non-preferential orientation present split diffraction peaks, meanwhile a preferential grown film in (001) orientation exhibit merged peaks describing as a pseudo-cubic perovskite structure.[29] However, this structural behavior is not observed in KNNe thin films shown in Fig. 1(b). The peak at $2\theta \sim 22°$ exhibits a slight split of the peak, which indicate the contribution of both (001) and (010) orientations, which is more evident at $2\theta \sim 45°$ and 70° (Fig. 1(b)).

On the other hand, KNNs films deposited with a stoichiometric commercial target consisting of the perovskite structure and the two secondary phases $K_4Nb_6O_{17}$ and $K_4Nb_6O_{17}$–$3H_2O$ (peaks marked by circles and triangles in the pattern, respectively). This is due to the volatilization of alkali cations promoting deficiency. In addition, the diffraction peaks of the $K_4Nb_6O_{17}$ phase are shifted towards higher angles, indicating a decrease of the lattice parameter b (Fig. 2(c)). This effect may be induced by the insertion of Na^+ in this secondary phase. The layered structure of $K_4Nb_6O_{17}$ has a coordination number of 8 for K^+ with ionic radii of 1.51 Å, while for Na^+ it is 1.18 Å,[30] thus reducing its lattice parameter.

3.2 Raman spectroscopy investigation

A couple structural study using Raman and XRD offers an ensure description due to their complementarity. In the experimental conditions of this work, XRD provides precise crystallographic data on phases, crystallinity, and lattice parameters for large-scale samples. Meanwhile, Raman spectroscopy delivers information about chemical bonding, orientation and nonuniform distortion of the crystal lattice on local microscale. Moreover, Raman has a high sensitivity of structural changes, allowing us to observe slight distortion of the cell or the presence of secondary phases possibly even if XRD patterns exhibit a single phase.

Raman characterization of six different areas and the deconvoluted spectra for KNNe (Fig. 2(a) and (b)) and KNNs (Fig. 2(c) and (d)) thin films were performed. The areas are illustrated in the film schematic in Fig. 2(f). According to earlier crystallographic studies, KNN exhibits the crystal space group $Amm2$ (C_{2v}^{14}) with Raman-active optical modes of $4A_1 + 4B_1 + 3B_2 + A_2$. These modes can be separated into translational modes of isolated cation (K^+ and Na^+) observed in the region before 200 cm^{-1}, and internal modes of coordination polyhedral (NbO_6).[11,31] NbO_6 octahedral vibrational modes are present in both KNN and $K_4Nb_6O_{17}$ phase, but with different arrangements. $K_4Nb_6O_{17}$ presents an orthorhombic $P2_1nb$ space group with shared NbO_6 octahedra at edges and vertices, separated by

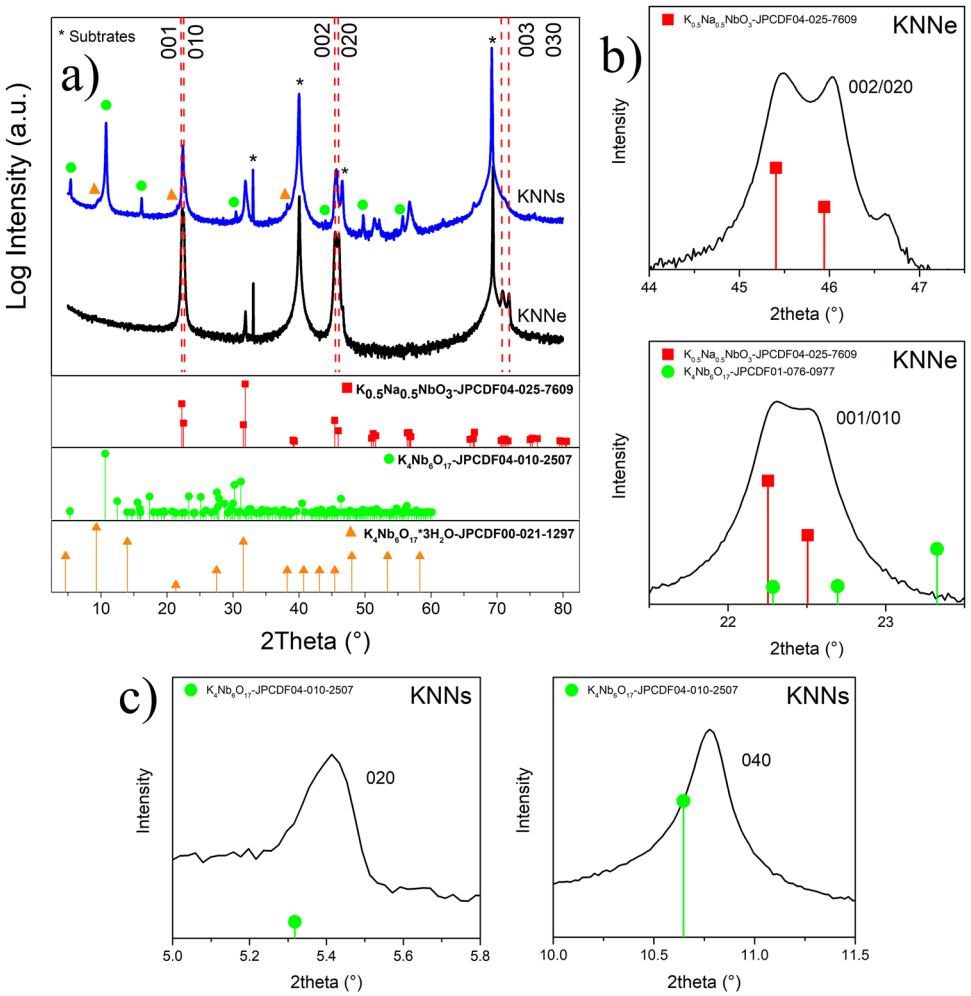

Fig. 1 (a) XRD patterns of KNNe and KNNs thin films obtained using an enriched target and a stoichiometric commercial target. In addition, reflection positions of the perovskite structure $K_{0.5}Na_{0.5}NbO_3$ (JPCDS 04-25-7609), and the secondary phases $K_4Nb_6O_{17}$ (JPCDS 04-010-2507) and $K_4Nb_6O_{17}$–$3H_2O$ (JPCDS 00-21-1297) are presented at the bottom of the patterns. Zoom in (b) of KNNe pattern between 2θ values from 21°–24° and 44°–47.5°, corresponding to the perovskite structure, and (c) of KNNs pattern between 2θ from 5°–5.8° and 10°–11.5°, corresponding to the secondary phase.

two types of potassium-filled interlayers.[13] In the literature, a study on single crystals of $K_4Nb_6O_{17}$ revealed weak peaks around 200–240 cm^{-1}, which get more intense for $K_4Nb_6O_{17}$–$3H_2O$ phase due to a partial depolarization induced by the intercalated water, as well as large peaks around 400 cm^{-1} and 900 cm^{-1} Raman shifts.[32] Furthermore, a study of nanocrystalline films and nano laminas of $K_4Nb_6O_{17}$ reports bands at 843, 877, 909 cm^{-1} for stretching mode of the shorter Nb–O bonds, and at 538, 584, 643 cm^{-1} for larger Nb–O bonds, as well as peaks between 200 to 480 cm^{-1} range assigned to bending vibrational modes of NbO_6 octahedra.[17,33] Raman spectra of KNNe films (Fig. 2(b)) obtained from an enriched target and KNNs films (Fig. 2(d)) obtained from a stoichiometric commercial target show the characteristic vibrational modes labeled ν_1, ν_2, ν_3, ν_4, ν_5, ν_6, $\nu_1 + \nu_5$ of the NbO_6 octahedra in the perovskite structure.[11,31] For KNNe thin films, spectra of all the analyzed areas confirm a single perovskite phase since no additional peaks were observed. However, KNNs thin films present two additional signals around 400 cm^{-1} and 878 cm^{-1}, which were increased from area 1 to 6. These signals were identified as vibrational modes of $K_4Nb_6O_{17}$, which agree with previous reports in thin films obtained by chemical solution deposition.[11,27,34] This explains the doublet peak in the region around 850–900 cm^{-1}, where there is an overlap between the NbO_6 signal from the perovskite around 843 cm^{-1} and the signal from the secondary phase $K_4Nb_6O_{17}$. In addition, multiple peaks in the 190–250 cm^{-1} range were observed in spectra from areas 5 and 6, which were associated to $K_4Nb_6O_{17}$ and $K_4Nb_6O_{17}$–$3H_2O$ (mark with green dots). The summary of the center and FWHM of Raman peaks for KNNe and KNNs thin films are in Table 2. Fig. 2(e) shows an example of Raman mapping typical of the bottom area of the sample with a color code indicating the intensity of the $K_4Nb_6O_{17}$ secondary phase in KNNs. The dark red spots represent the most intense secondary phase signal, while the dark blue spots are associated with a weaker signal. $K_4Nb_6O_{17}$ phase seems to be randomly spread across the entire probed zone without segregation. Therefore, it can be expected that KNNe films present

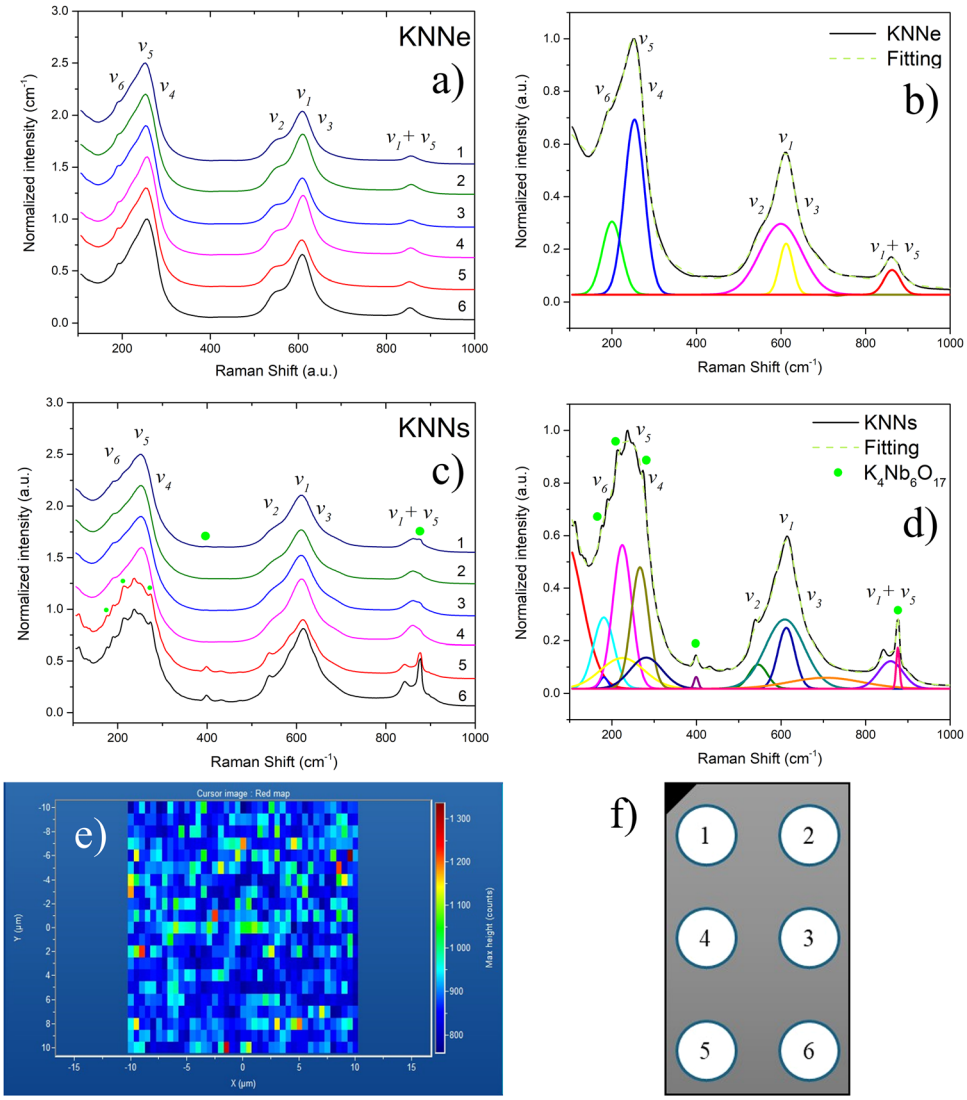

Fig. 2 Raman spectra mapping and deconvolution of (a) and (b) KNNe and (c) and (d) KNNs thin films obtained using an enriched target and a stoichiometric commercial target, respectively. (e) Raman mapping of KNNs recording in zone 5, the color code indicates an intense signal of the $K_4Nb_6O_{17}$ secondary phase in red and weak signal in blue. (f) Scheme of the thin film and the areas analyzed by Raman on a 10 × 20 mm^2 substrate.

Table 2 Summary of the center and FWHM of Raman peaks for KNNe and KNNs thin films

	ν_1 (cm^{-1})		ν_2 (cm^{-1})		ν_5 (cm^{-1})		ν_6 (cm^{-1})		$\nu_1 + \nu_5$ (cm^{-1})	
Thin film	Center	FWHM	Center	FWHM	Center	FWHM	Center	FWHM	Center	FWHM
KNNe	612	38	600	116	254	56	200	54	863	46
KNNs	609	108	546	51	225	52	181	57	859	68

strong homogeneous piezoelectric behavior through the sample, while KNNs thin films exhibit a weak behavior that may degrade along the films, according to the increment of the secondary phases.

3.3 SEM/EDXS

Fig. 3 shows the surface and cross-section SEM micrographs of the KNNe and KNNs thin films. The grain morphology of the films exhibits differences according to the target used. KNNe thin films obtained by a potassium enriched target presents round-like grains with 141 ± 33 nm average grain size (Fig. 3(a)), while KNNs films deposited with a stoichiometric commercial target show two different morphologies, small round-like grains with 93 ± 13 nm size and big cubic-like grains with 256 ± 55 nm (Fig. 3(c)). Corresponding histograms of the grain size distribution are shown as inset in Fig. 3(a) and (c). Cross-section micrographs show a dense columnar growth for both KNN thin films, the thickness for KNNe was 600 nm

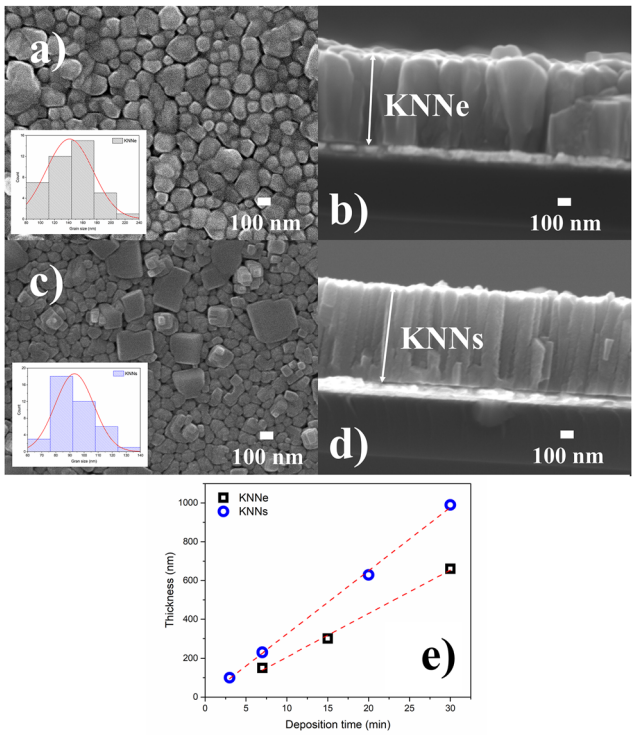

Fig. 3 Surface and cross-section SEM micrographs of (a) and (b) KNNe, and (c) and (d) KNNs thin films deposited using a K-enriched target and a stoichiometric commercial target, respectively. Histograms of the grain size distribution are shown as inset in each surface micrograph. (e) Deposition ratio of KNNe and KNNs thin films.

Table 3 Summary of compositional analysis performed by EDXS/SEM and cross-section of KNNe and KNNs thin films obtained by an enriched and stoichiometric commercial target, respectively

Sample	Average composition	Average grain size (nm)	Average thickness (nm)	Deposition rate (nm min^{-1})
KNNe	$(K_{0.57}Na_{0.43})_{1.12}NbO_3$	141 ± 33	600 ± 31	20 ± 1
KNNs	$(K_{0.54}Na_{0.46})_{0.87}NbO_3$	93 ± 13	660 ± 21	33 ± 2

(Fig. 3(b)), while KNNs thickness was 660 nm (Fig. 3(d)). This columnar growth was observed in another research works using PLD.[1,5] Table 3 summarizes the average grain size and thickness obtained using the software ImageJ. Rounded morphology, observed mainly in KNNe films, has been reported in previous works for KNN single perovskite phase. On the other hand, big cubic grains were identified previously in our research group as $K_4Nb_6O_{17}$ secondary phase.[22,23]

The EDXS analysis reveals a slight excess of alkali, $(K_{0.55}Na_{0.45})_{1.12}NbO_3$, for KNNe films, and an alkali cations deficiency for KNNs, $(K_{0.54}Na_{0.49})_{0.87}NbO_3$. This deficiency is caused by the volatilization of alkali cations, inducing secondary phases, such as $K_4Nb_6O_{17}$ and $K_4Nb_6O_{17}$–$3H_2O$, which were observed in XRD patterns. In contrast we have observed that a slight excess of alkali cations typically with an alkali/Nb ratio between 1.04 and 1.12 ensures the absence of secondary phases.

Furthermore, Fig. 3(c) shows the thickness of KNN thin films deposited at different durations. It is observed that the deposition rate is around 20 nm min^{-1} and 33 nm min^{-1} for KNNe and KNNs, respectively.[23] This difference is mainly attributed to the density of the targets. The enriched target has a density of approximately 60% with respect to KNN perovskite, which is lower than the commercial target with 97%. A high density offers more materials per volume, which increases the ablation rate. On the other hand, this behavior has been related to the small grain size, microcracks and lattice defects in the target, which facilitate the extraction of atomic-sized particles during the PLD process.[35] In addition to the target density, other parameters can influence the deposition rate, including target composition, laser fluence, target-substrate distance, background gas pressure and substrate temperature,[36] which were not investigated in this work.

3.4 TEM

Fig. 4 exhibits TEM micrographs and electron diffraction pattern of KNNs thin films deposited from the commercial stoichiometric target. Fig. 4(a) shows the TEM micrographs of five grains numerated from 1 to 5, the EDXS analysis of the grains are listed in Table 4. The grain 5 presents a close stoichiometric composition (alkali/Nb = 0.94), which can be identified as KNN perovskite phase. On the other hand, grains 1–4 show a deficiency in alkali cations in a range 0.62–0.85 alkali/Nb, which agree with SEM/EDXS analysis on larger scale. As mentioned in the XRD section, this deficiency is responsible for the formation of the $K_4Nb_6O_{17}$ phase according to the K_2O–Nb_2O_5 phase diagram.[12] However, grains 3 and 4, even though they present a similar total alkali ratio, their potassium and

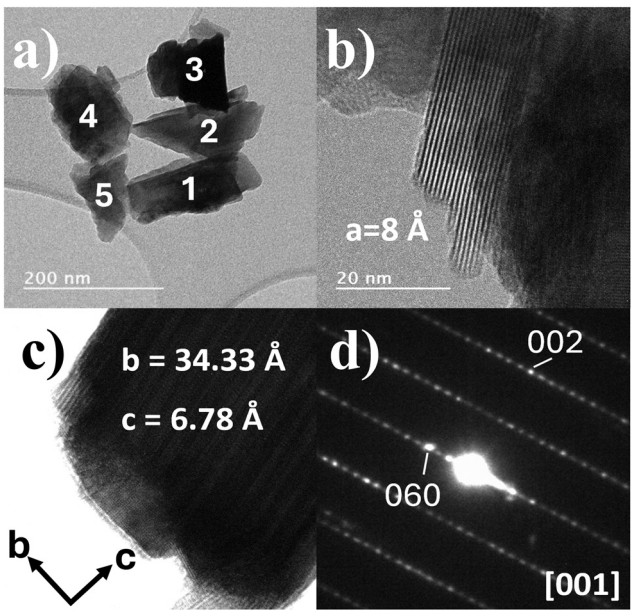

Fig. 4 (a) TEM micrograph of five grains from KNNs thin films deposited using a stoichiometric commercial target, which were analyzed by EDXS. (b) and (c) TEM images and (d) electron diffraction pattern of $K_4Nb_6O_{17}$ phase along the [001] zone axis.

Table 4 TEM/EDXS analysis for KNNs thin film

Grain	K	Na	Nb	(K + Na)/Nb
1	34.17	4.14	61.69	0.62
2	40.37	3.60	56.03	0.78
3	42.13	3.88	53.99	0.85
4	23.93	21.36	54.71	0.83
5	20.99	27.59	51.43	0.94

sodium content vary, suggesting different structures. In the case of grain 4, its stoichiometry is $(K_{0.53}Na_{0.47})_{0.83}$, showed to be associated here with the perovskite structure, in agreement with electron diffraction and with our previous works.[28,37] While grain 3 presents a large Na deficiency, this low solubility is characteristic of the lamellar $K_4Nb_6O_{17}$ secondary phase, as was observed in this work. So, it is important to highlight this slight presence of Na in grains 1–3 as a $K_{4-x}Na_xNb_6O_{17}$ solid solution not previously reported in $K_{0.5}Na_{0.5}NbO_3$ thin films. This insertion of Na^{1+} was also proposed in XRD analysis of KNNs thin films, where the peaks corresponding to the secondary phase are shifted toward larger angles due to a decrement in its lattice parameter. Fig. 4(b) presents a typical TEM micrograph of another grain. The *d* spacing measures ~8 Å, which corresponds to *a* lattice parameter of the orthorhombic phase of $K_4Nb_6O_{17}$. Fig. 4(c) and (d) shows a micrograph of a $K_4Nb_6O_{17}$ crystal, and the corresponding electron diffraction pattern indexed along the [001] zone axis. Well-defined diffraction spots are observed, indicating a high crystallinity. In addition, *d* spacings around 34.33 Å and 6.78 Å were determined, which agree with *b* and *c* lattice parameters of $K_4Nb_6O_{17}$.

3.5 Piezoresponse force microscopy

PFM measurements of KNNe and KNNs thin films were performed in different areas according to the scheme in Fig. 5. The amplitude response of KNNe (Fig. 5(a) and (c)) is typical of a layer whose all grains are piezoelectric, leading to a strong (bright) contrast all over the surface and well-defined grain boundaries (visible on Fig. 5(b), where the scale is smaller compared to other images: grain boundaries appear as dark thin lines that surround grains). Meanwhile, the response of KNNs films is not homogeneous, and the percentage of grains showing a piezoelectric activity is not the same depending on the studied area. From region A to C, fewer and fewer piezoelectric areas are detected. In Fig. 5(f), a very small percentage of the total area shows a piezoelectric response. These results agree with Raman spectroscopy investigation, where six different areas in the films were analyzed, observing that $K_4Nb_6O_{17}$ secondary phase signal increased from area A to F, according to the thin film scheme in Fig. 2(f). In addition, the compositional analysis by EDXS/SEM showed a deficiency on alkali cations, which promotes the formation of the $K_4Nb_6O_{17}$ secondary phase. Moreover, Fig. 6(a)–(f) presents the topography (error signal), PFM amplitude and phase images of KNNe and KNNs thin films from a 2 × 2 μm² area. KNNe films present a highly polydomain surface with domains' frontier clearly visible, and high roughness around 8.6 nm RMS (Fig. 6(a)–(c)). KNNs films exhibit some flat grains (enclosed in white circles) with a dark contrast in amplitude image, which indicate non-piezoelectric response (Fig. 6(d)–(f)). All piezoelectric grains in KNNs films seem to be oriented in the same way: apart from the non-piezoelectric regions where the phase PFM signal is noisy, only one sense of polarization can be detected contrary to KNNe, where both polarities can be easily found (dark and bright zones in the PFM phase image).

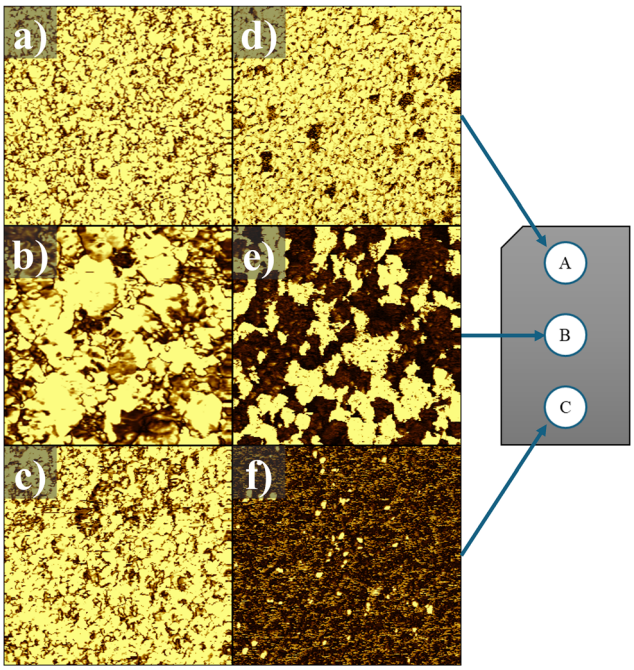

Fig. 5 PFM vertical amplitude images in different areas of KNNe (a)–(c) and KNNs (d)–(f) thin films using an enriched target and a stoichiometric commercial target, respectively: (a) and (d) top, (b) and (e) center, (c) and (f) down. Bright zones indicate large piezoelectric activity (all images 5 × 5 μm², except (b) 2 × 2 μm², where domain boundaries are visible).

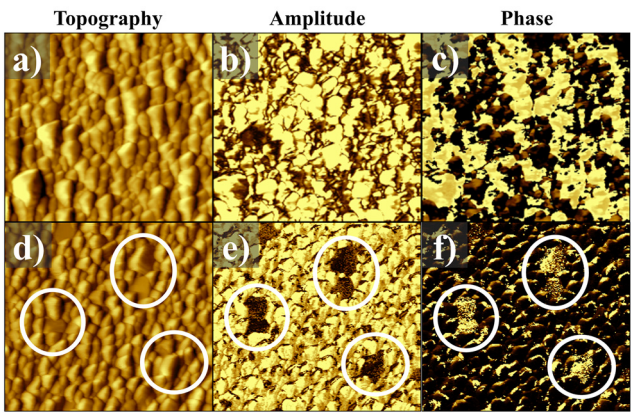

Fig. 6 Topography, amplitude and phase images from 2 × 2 μm² area of (a)–(c) KNNe and (d)–(f) KNNs thin films obtained using an enriched target and a stoichiometric commercial target, respectively. White circles enclose flat grains, which present nonpiezoelectric response.

3.6 Electrical characterization

Ferroelectric and piezoelectric measurements were performed on capacitors of 0.25 × 0.25 mm^2 in area, based on both KNNe and KNNs thin films. Fig. 7(a) and (b) shows the ferroelectric hysteresis loops and the associated current measured with a triangular bipolar signal (10 V, 3 kHz). KNNe film shows typical hysteresis shape characteristic of ferroelectric material. The maximum polarization reaches 20 μC cm^{-2} for an applied voltage of 10 V, while the remnant polarization ($2P_r$) and coercive voltage ($2V_c$) are 17.5 μC cm^{-2} and 3 V, respectively. On the contrary, KNNs film does not show obvious ferroelectric behavior. The measured polarization-voltage loops are systematically more or less inflated so that we do not clearly see the two current peaks corresponding to dipoles switching on current–voltage curves, like KNNe. Moreover, the current increases dramatically under high voltage. In the worst case, where the secondary phase is abundant, like at the bottom of the sample (film scheme in Fig. 5 region C), the capacitors appear more often in short circuit, which agree with PFM results illustrated in Fig. 5(e) and (f) where the piezoelectric areas gradually disappeared. We thus assume a possible correlation between the presence of $K_4Nb_6O_{17}$ phase and the leaky behavior of the film. Indeed, it has already been reported that high conductivity in non-stoichiometric KNN film can result from the presence of secondary (hygroscopic) phases, thus like $K_4Nb_6O_{17}$ in our case.[38] Fig. 7(c) shows the large-signal displacement response of the KNN films measurement with the DBLI. Both films show the butterfly loop characteristics of ferroelectric domain switching. However, KNNe films presents higher displacement than KNNs counterpart. The $d_{33,f}$ coefficient obtained by fitting the slope of wings in the displacement loop reaches ~40 pm V^{-1} for KNNe and ~30 pm V^{-1} for KNNs. We can notice that the properties of our KNNe film are quite similar to those reported by M. D. Nguyen, *et al.*,[1] which is also a PLD deposited KNN 50/50 on platinized silicon substrate.

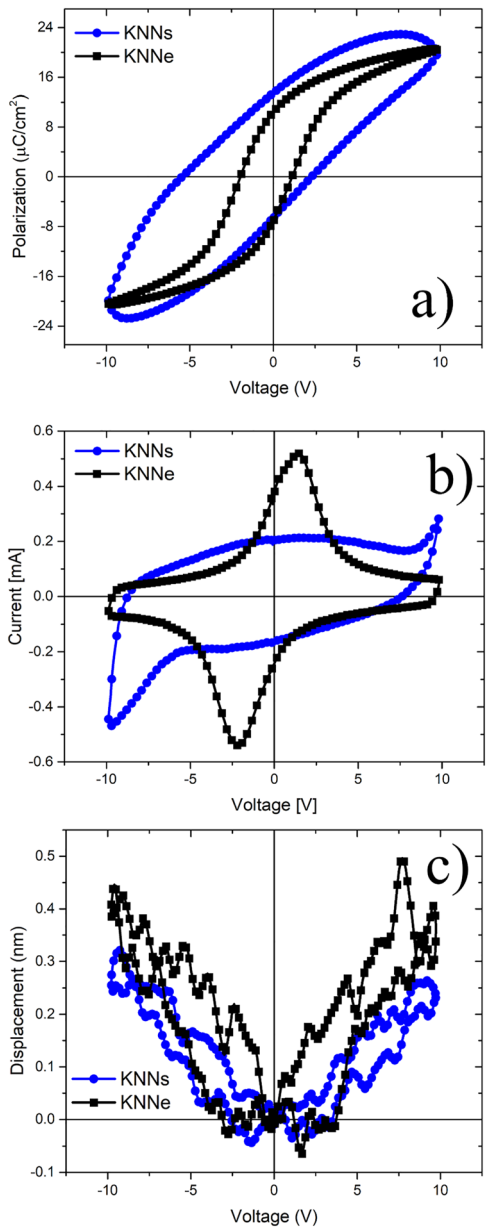

Fig. 7 (a) Ferroelectric hysteresis loops (b) current curves and (c) displacement response of KNNe and KNNs thin films at 3 kHz and 10 V.

4. Conclusions

The influence of the secondary phase $K_4Nb_6O_{17}$ on piezoelectric and ferroelectric KNN thin films deposited with stoichiometric and K-enriched targets was studied. It was observed that good stoichiometric control of KNN thin films is possible by adding an excess of 60% mol K into the target to compensate for alkali cation losses during PLD deposition, such as KNNe thin films. On the contrary, KNNs films obtained by a stoichiometric target present alkali deficiency, which promotes mainly the formation of secondary phase $K_4Nb_6O_{17}$ and due to its highly sensitivity to moisture, $K_4Nb_6O_{17}$–$3H_2O$ phase was formed. It is worth noticing that such secondary phases can form easily even for quite low alkali deficiency typically ~0.83 mol, as was observed in this work. In addition, the secondary phase $K_4Nb_6O_{17}$ presented a slight shift in its characteristics X-ray diffraction peaks suggesting a shrink of their lattice parameters due to the incorporation of sodium in its structure. This finding was validated by analyzing their compositional and structural characteristics by TEM/EDXS, corroborating a slight solubility of sodium into the secondary phase $K_4Nb_6O_{17}$, which has not been reported previously. Therefore, one cause of the high field conductivity in KNN is the presence of secondary hygroscopic phases that result from non-stoichiometry, due to the alkali loss during the deposition process, while the use of K-excess into the target ensures strong ferroelectric and piezoelectric behavior ($2P_r$ and $d_{33,f}$ are 17.5 μC cm^{-2} and ~40 pm V^{-1}, respectively).

Author contributions

B. Carreño-Jiménez: conceptualization, investigation, formal analysis, writing – original draft, visualization. H. Kuentz:

conceptualization, investigation, formal analysis, review & editing. K. Kpoton: conceptualization, investigation, formal analysis, review & editing. T. Rotrou: investigation, review & editing. S. Ollivier: investigation. V. demange: conceptualization, investigation, formal analysis, writing – review & editing. L. Joanny: investigation. L. Rault: investigation, review & editing. G. Taupier: conceptualization, investigation, formal analysis, review & editing. B. Gautier: conceptualization, investigation, writing – review & editing, funding acquisition. G. Le Rhun: conceptualization, investigation, writing – review & editing, funding acquisition. M. Guilloux-Viry: conceptualization, investigation, resources, supervision, writing – review & editing, visualization, project administration, funding acquisition.

Conflicts of interest

There are no conflicts to declare.

Data availability

The data supporting this article are publicly available on Zenodo (648.8 kB) (**https://doi.org/10.5281/zenodo.16369997**).

Acknowledgements

Authors acknowledge the French National Research Agency (ANR abbreviation in French) for the financial support in the project ''Towards and Industry compatible high performance Lead-free Piezoelectric thin film material for MEMS ACtuators applications (TILPAC)'' No. ANR-22-CE08-0017. The SEM, TEM, EDXS and Raman spectrometry characterizations were performed using facilities platforms of UAR ScanMAT (Platforms CMEBA, THEMIS and SIR). Dr Alain Moreac is warmly thanked for his advice on Raman spectrometry. We also thank Mathieu Bernard for the KNN commercial target.

References

1 M. D. Nguyen, M. Dekkers, E. P. Houwman, H. T. Vu, H. N. Vu and G. Rijnders, Lead-free $(K_{0.5}Na_{0.5})NbO_3$ thin films by pulsed laser deposition driving MEMS-based piezoelectric cantilevers, *Mater. Lett.*, 2016, **164**, 413–416, DOI: **10.1016/j.matlet.2015.11.044**.

2 H. Kuentz, C. Dieppedale, L. Mollard, R. Liechti, A. Campo, A. Hamelin, V. Demange, C. Poulain, M. Guilloux-Viry and G. Le Rhun, KNN lead-free technology on 200 mm Si wafer for piezoelectric actuator applications, *Sens. Actuators, A*, 2024, **372**, 115370, DOI: **10.1016/j.sna.2024.115370**.

3 K. Shibata, K. Watanabe, T. Kuroda and T. Osada, KNN lead-free piezoelectric films grown by sputtering, *Appl. Phys. Lett.*, 2022, **121**, 092901, DOI: **10.1063/5.0104583**.

4 G. Shirane, R. Newnham and R. Pepinsky, Dielectric Properties and Phase Transitions of $NaNbO_3$ and $(Na,K)NbO_3$, *Phys. Rev.*, 1954, **96**, 581–588, DOI: **10.1103/PhysRev.96.581**.

5 I. Fujii, S. Tagata1, T. Nakao1, N. Koyama1, H. Adachi and T. Wada, Fabrication of $(K,Na)NbO_3$ films on $SrRuO_3$/$(001)SrTiO_3$ substrates by pulsed laser deposition, *Jpn. J. Appl. Phys.*, 2015, **54**, 10NA13, DOI: **10.1063/1.4823852**.

6 Y. Wang, K. Yao, M. S. Mirshekarloo and F. E. H. Tay, Effects and Mechanism of Combinational Chemical Agents on Solution-Derived $K_{0.5}Na_{0.5}NbO_3$ Piezoelectric Thin Films, *J. Am. Ceram. Soc.*, 2016, **99**, 1631–1636, DOI: **10.1111/jace.14139**.

7 D. Zhangab, F. Zhenga, X. Yanga, L. Fenga, X. Huanga, H. Liuc and M. Cao, Preparation and ferroelectric properties of $K_{0.5}Na_{0.5}NbO_3$ thin films derived from non-alcohol niobium salt sol–gel process, *Integr. Ferroelectr.*, 2014, **154**, 97–102, DOI: **10.1080/10584587.2014.904166**.

8 R. Castañeda-Guzmán, R. López-Juárez, J. J. Gervacio, M. P. Cruz, S. Díaz de la Torre and S. J. Pérez-Ruiz, Structural and piezo-ferroelectric properties of $K_{0.5}Na_{0.5}NbO_3$ thin films grown by pulsed laser deposition and tested as sensors, *Thin Solid Films*, 2017, **636**, 458–463, DOI: **10.1016/j.tsf.2017.06.039**.

9 A. Tian, W. Ren, L. Wang, H. Du and X. Yao, Effects of deposition temperature on structure and properties of $(K_{0.48}Na_{0.52})$-NbO_3 ferroelectric thin films by pulsed laser deposition, *J. Appl. Phys.*, 2013, **114**, 134103, DOI: **10.1063/1.4823852**.

10 K. N. Pham, N. H. Gaukas, M. Morozov, T. Tybell, P. E. Vullum, T. Grande and M. Einarsrud, Epitaxial $K_{0.5}Na_{0.5}NbO_3$ thin films by aqueous chemical solution deposition, *R. Soc. Open Sci.*, 2019, **6**(1), 180989, DOI: **10.1098/rsos.180989**.

11 W. Ahn, H. I. Hwang, K. Sei Lee, B. Moon Jin, S. Park, G. Park, D. Yoon, H. Cheong, H. Joon Lee and I. Won Kim, Raman spectra study of $K_{0.5}Na_{0.5}NbO_3$ ferroelectric thin films, *Jpn. J. Appl. Phys.*, 2010, **49**, 095801, DOI: **10.1143/JJAP.49.095801**.

12 R. Blachnik and E. Irle, Das System $KNbO_3$-Nb_2O_5, *J. Therm. Anal.*, 1989, **35**, 609–615, DOI: **10.1007/BF01904462**.

13 M. Gasperin and M. T. Le Bihan, Mecanisme d'hydratation des niobates alcalins lamellaires de formule $A_4Nb_4O_{17}$ (A = K, Rb, Cs), *J. Solid State Chem.*, 1982, **43**, 346–353, DOI: **10.1016/0022-4596(82)90251-1**.

14 G. Du, Q. Chen, Y. Yu, S. Zhang, W. Zhou and L.-M. Peng, Synthesis, modification and characterization of $K_4Nb_6O_{17}$-type nanotubes, *J. Mater. Chem.*, 2004, **14**, 1437, DOI: **10.1039/b317095k**.

15 G. M. Loiacono and B. Michelman, Growth and properties of $K_4Nb_6O_{17}$, *J. Am. Ceram. Soc.*, 1968, **51**, 542–543.

16 H. Kimura, R. Tanahashi, H. Zhao and Q. Yao, Weak ferroelectricity of potassium niobate $K_4Nb_6O_{17}$ single crystal grown by pulling down technique, *Mater. Lett.*, 2012, **84**, 16–19, DOI: **10.1016/j.matlet.2012.06.052**.

17 Q. Deng, M. Li, J. Wang, P. Zhang, K. Jiang, J. Zhang, Z. Hu and J. Chu, Exploring optoelectronic properties and mechanisms of layered ferroelectric $K_4Nb_6O_{17}$ nanocrystalline films and nanolaminas, *Sci. Rep.*, 2017, **7**, 1–13, DOI: **10.1038/s41598-017-01838-6**.

18 S. K. Sahu, L. A. Boatner and A. Navrotsky, Formation and Dehydration Enthalpy of Potassium Hexaniobate, *J. Am. Ceram. Soc.*, 2017, **100**, 304–311, DOI: **10.1111/jace.14465**.

19 P. Pop-Ghe, N. Wolff, A. Rubab, L. Kienle and E. Quandt, Tailoring growth modes by excess alkali addition in magnetron sputtered potassium sodium niobate thin films, *Mater. Today Commun.*, 2021, **27**, 102221, DOI: 10.1016/j.mtcomm.2021.102221.

20 S. Sharma, A. Kumar, V. Gupta and M. Tomar, Dielectric and ferroelectric studies of KNN thin film grown by pulsed laser deposition technique, *Vacuum*, 2019, **160**, 233–237, DOI: 10.1016/j.vacuum.2018.11.036.

21 C. W. Ahn, S. Y. Lee, H. J. Lee, A. Ullah, J. S. Bae, E. D. Jeong, J. S. Choi, B. H. Park and I. W. Kim, The effect of K and Na excess on the ferroelectric and piezoelectric properties of $K_{0.5}Na_{0.5}NbO_3$ thin films, *J. Phys. D: Appl. Phys.*, 2009, **5–10**(42), 215304, DOI: 10.1088/0022-3727/42/21/21530442.

22 W. T. Hicks, Evaluation of vapor-pressure data for mercury, lithium, sodium, and potassium, *J. Chem. Phys.*, 1963, **38**, 1873–1880, DOI: 10.1063/1.1733889.

23 H. Kuentz, *Couches minces piézoélectriques sans plomb pour l'actionnement et fiabilité*, Université de Rennes, 2024, https://theses.fr/2024URENS073.

24 B. Aspe, F. Cissé, X. Castel, V. Demange, S. Députier, S. Ollivier, V. Bouquet, L. Joanny, R. Sauleau and M. Guilloux-Viry, $K_xNa_{1-x}NbO_3$ perovskite thin films grown by pulsed laser deposition on *R*-plane sapphire for tunable microwave devices, *J. Mater. Sci.*, 2018, **53**, 13042–13052, DOI: 10.1007/s10853-018-2593-9.

25 M. S. Bradley, Lineshapes in IR and Raman spectroscopy: A primer, *Spectrosc.*, 2015, **30**, 42.

26 M. Zannen, A. Lahmar, M. Dietze, H. Khemakhem, A. Kabadou and M. Es-Souni, Structural, optical, and electrical properties of Nd-doped $Na_{0.5}Bi_{0.5}TiO_3$, *Mater. Chem. Phys.*, 2012, **134**, 829–833, DOI: 10.1016/j.matchemphys.2012.03.076.

27 V. T. Hien and N. T. Minh Phuong, Microstructure and Electrical Properties of Low-temperature Solution-processed Sol-gel KNN Thin Films, *VNU J. Sci.: Math. – Phys.*, 2020, **36**, 58–65, DOI: 10.25073/2588-1124/vnumap.4460.

28 A. Waroquet, V. Demange, N. Hakmeh, J. Perrière, S. Freslon, S. Députier and M. Guilloux-Viry, Epitaxial growth and cationic exchange properties of layered KNb_3O_8 thin films, *RSC Adv.*, 2017, **7**, 15482–15491, DOI: 10.1039/c7ra00261k.

29 K. Shibata, K. Suenaga, K. Watanabe, F. Horikiri, T. Mishima and M. Shiratani, Evaluation of Crystal Orientation for (K,Na)NbO_3 Films Using X-ray Diffraction Reciprocal Space map and relationship between crystal orientation and piezoelectric coefficient, *Jpn. J. Appl. Phys.*, 2012, **51**, 075502, DOI: 10.1143/JJAP.51.075502.

30 R. D. Shannon, Revised Effective Ionic Radii and Systematic Studies of Interatomie Distances in Halides and Chaleogenides Central Research and Development Department, Experimental Station, E. L. Du Pont de Nemours and Company Wilmington, Delaware 19898, U.S.A, *Acta Crystallogr.*, 1976, **A32**, 751–767, DOI: 10.1107/s0567739476001551.

31 K. I. Kakimoto, K. Akao, Y. Guo and H. Ohsato, Raman scattering study of piezoelectric $(Na_{0.5}K_{0.5})NbO_3$-$LiNbO_3$ ceramics, *Jpn. J. Appl. Phys., Part 1*, 2005, **44**, 7064–7067, DOI: 10.1143/JJAP.44.7064.

32 M. Mączka, M. Ptak, A. Majchrowski and J. Hanuza, Raman and IR spectra of $K_4Nb_6O_{17}$ and $K_4Nb_6O_{17}{\cdot}3H_2O$ single crystals, *J. Raman Spectrosc.*, 2011, **42**, 209–213, DOI: 10.1002/jrs.2668.

33 M. A. Bizeto, F. Leroux, A. L. Shiguihara, M. L. A. Temperini, O. Sala and V. R. L. Constantino, Intralamellar structural modifications related to the proton exchanging in $K_4Nb_6O_{17}$ layered phase, *J. Phys. Chem. Solids*, 2010, **71**, 560–564, DOI: 10.1016/j.jpcs.2009.12.036.

34 X. Vendrell, O. Raymond, D. A. Ochoa, J. E. García and L. Mestres, Growth and physical properties of highly oriented La-doped (K,Na)NbO_3 ferroelectric thin films, *Thin Solid Films*, 2015, **577**, 35–41, DOI: 10.1016/j.tsf.2015.01.038.

35 Y. Kim, F. Mitsugi, T. Ueda and T. Ikegami, Characteristics of ZnO thin films fabricated by shock-consolidated ZnO target, *Ceram. Int.*, 2011, **37**, 2921–2925, DOI: 10.1016/j.ceramint.2011.05.076.

36 K. Bin Masood, P. Kumar, M. A. Malik and J. Singh, A comprehensive tutorial on the pulsed laser deposition technique and developments in the fabrication of low dimensional systems and nanostructures, *Emergent Mater.*, 2021, **4**, 737–754, DOI: 10.1007/s42247-020-00155-5.

37 B. Aspe, V. Demange, A. Waroquet, X. Castel, B. Gautier, Q. Simon, D. Albertini, M. Zaghrioui, K. Nadaud, S. Députier, F. Gouttefangeas, R. Sauleau and M. Guilloux-Viry, Tetragonal tungsten bronze phase thin films in the K–Na–Nb–O system: Pulsed laser deposition, structural and dielectric characterizations, *J. Alloys Compd.*, 2020, **827**, 1–11, DOI: 10.1016/j.jallcom.2020.154341.

38 V. Kovacova, J. I. Yang, L. Jacques, S. W. Ko, W. Zhu and S. Trolier-McKinstry, Comparative Solution Synthesis of Mn Doped (Na,K)NbO_3 Thin Films, *Chem. – Eur. J.*, 2020, **26**, 9356–9364, DOI: 10.1002/chem.202000537.